FEBS Letters 579 (2005) 1968–1972 FEBS 29391

Structural basis of gating of CNG channels

Alejandro Giorgetti[1], Anil V. Nair, Paolo Codega, Vincent Torre, Paolo Carloni*

Istituto Nazionale per la Fisica della Materia (INFM – DEMOCRITOS Modeling Center for Research In aTOmistic Simulation) and International School for Advanced Studies (SISSA), Via Beirut 4, 34014 Trieste, Italy

Received 14 December 2004; revised 24 January 2005; accepted 28 January 2005

Available online 2 March 2005

Edited by Maurice Montal

Abstract **Cyclic nucleotide-gated (CNG) ion channels, underlying sensory transduction in vertebrate photoreceptors and olfactory sensory neurons, require cyclic nucleotides to open. Here, we present structural models of the tetrameric CNG channel pore from *bovine rod* in both open and closed states, as obtained by combining homology modeling-based techniques, experimentally derived spatial constraints and structural patterns present in the PDB database. Gating is initiated by an anticlockwise rotation of the N-terminal region of the C-linker, which is then, transmitted through the S6 transmembrane helices to the P-helix, and in turn from this to the pore lumen, which opens up from 2 to 5 Å thus allowing for ion permeation. The approach, here presented, is expected to provide a general methodology for model ion channels and their gating when structural templates are available and an extensive electrophysiological analysis has been performed.**

Keywords: CNG channels; Gating mechanism; Comparative modelling; Structural basis; Distance restraints

Ion channels are membrane spanning proteins that allow ions, such as K^+, Na^+, Ca^{2+} and Cl^-, to cross the hydrophobic core of the cell membrane [1]. Because of the well-known difficulties in obtaining high resolution 3D structures by X-ray crystallography of ion channels, alternative strategies based on computational biology tools are currently used to investigate their biophysical properties (for reviews on ion channel modelling see: [2–4]).

Here, we present a computational structural study on the widely characterized homotetrameric cyclic nucleotide-gated channel (CNG), from *bovine rod*, composed by the subunit CNGA1 [5], which forms functional assemblies with the same selectivity and gating properties as the native channels, which are instead heteromeric tetramers. Each subunit consists of two domains: (i) a transmembrane domain formed by six transmembrane helices (S1–S6) and a pore helix (P-helix) with the same topology of voltage-gated K^+ channels [6,7]. (ii) A cytoplasmic domain formed by the cyclic nucleotide binding domain (CNBD) which is linked to the transmembrane domain through the so called C-linker region. The pore, unselective for Na^+ and K^+, is believed to gate via a conformational change of S6 transmembrane helix (TMH) initiated by the binding of cyclic nucleotides to the binding domains. This conformational change is transduced to the pore via coupling with the four P-helices [8,9].

Here, we provide a molecular basis to this proposal by constructing models of the transmembrane region of the CNGA1 channel from *bovine rod*, which includes S6, P-helix-loop (P-helix + pore wall or filter), along with the C-linker N-terminal section, for which there exist a great amount of experimental data. Models of P-helix-loop and S6 are based on the KcsA X-ray structure [10,11], whose topology has been suggested to be similar to that of CNG channels [6]. The C-linker domain was modeled using the C-linker of the HCN (from *mouse*) channel in ligand bound state, for which the X-ray structure has been recently solved [12]. This template shares a high sequence identity (>30%) with CNG channels in this particular region. Finally, the obtained models refer to residues from Arg345 to Arg422 of the CNGA1 channel.

The models, obtained based on the alignments shown in Fig. 1A, were refined by the inclusion of an extensive dataset of spatial constraints inferred by electrophysiological measurements on cysteine mutants (Fig. 1B and C). A large set (about 50) of structural constraints among Cα atoms are inferred from measurements in the presence of metal ions (Table 1) [6,13–20]: (i) Cd^{2+}, which can block the channel [21] when it binds to, at least, two cysteine residues (see Table 1). Estimates obtained by a calculation of residue–residue distribution function based on the RCSB Protein Data Bank [22] suggest that the Cα of these cysteines are located at about 11–13 Å (Fig. 1D and the Note in the figure caption) [23]. (ii) Mild-oxidizing agent copper phenanthroline (CuP) favors disulfide bridge formation between two cysteines separated by a distance going from 6 to 11 Å (see Fig. 1D and the Note in the figure caption).

A smaller set of data (about 20) provide information on solvent accessibilities, inferred from measurements in the presence of three differently sized and charged sulfhydryl specific reagents such as $MTSET^+$, $MTSEA^+$ and $MTSES^-$. Indeed, these compounds may react with solvent accessible cysteines [24] (Table 1) [25].

In the S6 TMH and in the N-terminal portion of the C-linker, Cd^{2+} blockage is almost absent for residues upstream Gly395 in both open and closed states, whilst it is strongly state dependent for residues downstream Asn400 (Table 1 and Fig. 1C). As a result, in the open state, the N-terminal section of the C-linker is bent around a hinge located approximately between Val391 and Gly395, and it is also rotated in the anticlockwise sense by about 60° (around the helix axis) related to the closed conformation, assuming a configuration similar to that of the template (Fig. 2). These conformational changes resemble somehow that proposed for the Shaker K^+ channel [26], in

*Corresponding author.
E-mail address: carloni@sissa.it (P. Carloni).

[1] Present address: Department of Biochemical Sciences, University of Rome "La Sapienza".

0014-5793/$30.00
doi:10.1016/j.febslet.2005.01.086

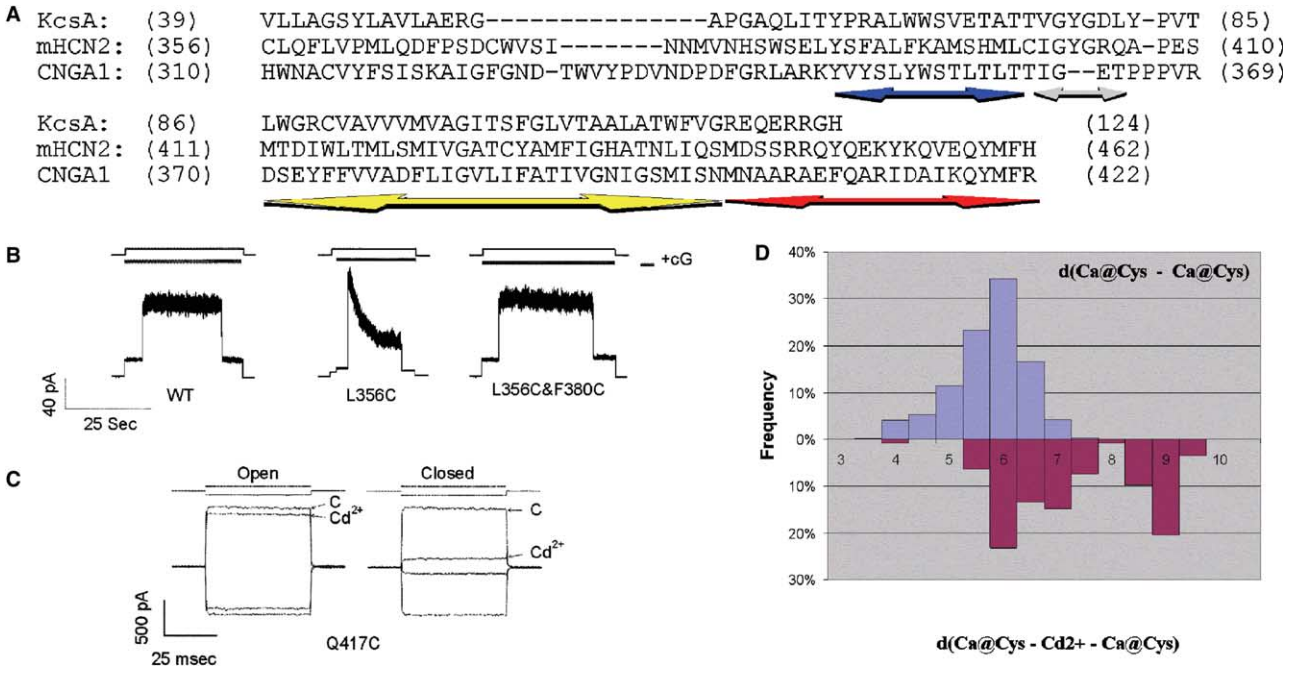

Fig. 1. (A) Sequence alignment of the CNGA1 channel from bovine rod used for building up the structure by homology modelling. The templates are: KcsA K^+ channel from *Streptommyces lividans* [11,30] for P-helix-loop and TM2/S6, and HCN from *mouse* for the C-linker [12]. Colour coding (for all figures): Gray: pore walls (filter). Blue: P-helix. Yellow: S6 transmembrane helix. Red: C-linker N-terminal section. Selected experiments taken from [18,19]: (B) Current response for wild type (wt), mutant L356C and double mutant L356C & F380C in the presence of 1 mM cGMP (cG). L356C desensitise while double mutant shows similar response like wt. (C) Effect of 100 μM Cd^{2+} in the open and closed states of mutant Q417C (C: control current; Cd^{2+} is the current after cadmium application for 5 min). (D) Distances between Cα of cysteines forming disulfide bridges or coordinating to Cd^{2+} ions (blue and red, respectively). Distributions were obtained by screening of the PDB data bank [22]. For the latter distance, note that there are two distributions (from 4 to 7.5 and 8.5–10 Å) associated to complexes involving two adjacent and opposite cysteine residues, respectively. Note: In the used distance restraints (see text and Table 1) an average of 2.5–3 Å was added, in order to consider thermal fluctuations.

which the S6 TMH bends around a valine residue (Val374). This residue is in correspondence to CNG's Val391, suggesting a common mechanism in the gating of a variety of ion channels.

In the P-helix-loop region, formed by the P-helix and the putative filter region (known also as the pore walls), the following structural features can be established.

In the P-helix, L356 forms hydrophobic interactions with F380@S6. In fact, L356C desensitizes and F380C shows locking effects, whilst L356C & F380C double mutant (Table 1 and Fig. 1B) behaves as wt, suggesting that in the latter case the hydrophobic interactions are substituted by an S–S bridge (Fig. 2). In addition, this helix changes its location in space on passing from closed to open form. Indeed, Thr355 and Leu358 of the P-helix are accessible to extracellular solvent only in the closed state, whilst Val348 and Leu351 are accessible in both states (Table 1).

For the filter, we notice that: (i) the homology of the sequences here is very low (Fig. 1). (ii) The filter GYG motif for K^+ channels is *not* conserved in CNG channels (Fig. 1), as the Tyr residue and one Gly residue have been lost during evolution. Thus, there must be two gaps on passing from the K^+ channel sequence to that of the CNG channel. As a result, the accuracy in this region is clearly very low and the only structural information should come from experimental data [13]. Specifically, it is found that Thr360 is solvent accessible in both states and this residue exhibits different conformation in the open and closed conformation, as shown by the differences in response upon Cd^{2+} addition (Table 1): In the open state, the channel is blocked by Cd^{2+}, and thus the distance between the T360C's Cα should be of about 11–13 Å (Table 1), whilst in the closed state it is not blocked, so this distance should be larger than 14 Å. The experimental data on Thr360 have immediate consequences on the conformation of the adjacent residues Ile361 and Gly362: in both cases, the distances between Cα belonging to opposite subunits increase in passing from the closed to the open conformation (e.g. distance between opposite Gly362 Cα increases from 3 to about 6 Å, Fig. 2), making the pore lumen to increase upon opening, till a diameter of about 5 Å. Although the difficulties in modelling and the low accuracy found in this region, this result, and in particular the variation of the pore lumen obtained in the models (Fig. 2), is corroborated by measurements based on the permeability of the channel to large organic cations (such as NH_4^+, $CH_3NH_3^+$, $(CH_3)_2NH_2^+$, $(CH_3)_3NH^+$ and $CH_2CH_3NH_3^+$) [27–29]: using permeability information, it was possible to estimate that the diameter of the narrowest part of bovine CNG channel pores in the open configuration measures between 4 and 6 Å [27–29].

On the basis of these findings, we propose that gating occurs by bending and an anticlockwise rotation by about 60° (around the helix axis and seen from the extracellular side of the membrane) of the C-linker N-terminal section (Fig. 2). This rotation is transmitted upwards, making the upper part of S6 to rotate anticlockwise by about 30° (around the helix axis). Due to the direct interaction of S6 with the P-helix, this motion is transmitted to the latter, which rearranges so as its terminal Thr360 residues and therefore, the lower part of the pore wall, leading to the opening of the pore lumen.

Table 1
Spatial constraints involving P-helix-loop, S6 and N-term@C-linker of CNGA1 channels from bovine rod, based on experimental data on cysteine mutants

Mutant	Cd^{2+}		MTS		Restraint
	Open	Closed	Open	Closed	
V348C	Block-E NoEff-I [20]	Block-E NoEff-I [20]	Block-MTSET-E [6,13]	Block-MTSET-E [6,20]	Accessible from outside open/closed state
	–	–	NoEff-MTSET-E [13]	NoEff-MTSET-E [13]	
S350C	NoEff E&I [16]	NoEff E&I [16]	NoEffMTSET-E [13]	NoEff-MTSET-E [13]	
L351C	–	–	**NoEff-MTSET-E** [20]	**Block-MTSET-E** [20]	Accessible from outside closed state
Y352C	–	–	NoEff-MTSET-E [6]	NoEff-MTSET-E [13]	
W353C	–	–	NoEff-NTSET-E [6]	NoEff-MTSET-E [13]	
S354C	–	–	NoEff-MTSET-E [6]	NoEff-MTSET-E [13]	
T355C	–	–	**NoEff-MTSET-E** [6]	**Block-MTSET-E** [13]	Accessible from outside closed state
L356C	–	–	NoEff-MTSET-E [6]	NoEff-MTSET-E [13]	
T357C	–	–	NoEff-MTSET-E [6]	NoEff-MTSET-E [13]	
L358C	–	–	**NoEff-MTSET-E** [20]	**Block-MTSET-E** [13]	Accessible from outside closed state
T359C			NoEff-MTSET-E [13]	NoEff-MTSET-E [13]	
T360C	**Block-I** [20]	**NoEff-I** [20]	Poten-MTSES-I [18]	Poten-MTSES- I [18]	D(Cα–Cα) ≈ 11 Å (open) D(Cα–Cα) > 14 Å (closed) Accessible from inside
I361C	Block-I [20]	Block-I [20]	NoEff-MTSET-E [13]	NoEff-MTSET-E [13]	Accessible from inside
G362C	–	–	NoEff-MTSET-E [13]	NoEff-MTSET-E [13]	
E363C	–	–	Block-MTSET-E [13]	Block-MTSET-E [13]	Accessible from outside open/closed-state
T364C	Block-E NoEff-I [20]	Block-E NoEff-I [20]	Block-MTSET-E NoEff-MTSET-I [6,13]	Block-MTSET-E NoEff-MTSET-I [6,13]	Accessible from outside open/closed-state
P365C	–	–	NoEff-MTSET-E,I [6]	NoEff-MTSET-E,I [6]	
P366C	Block-E NoEff-I [20]	Block-E NoEff-I [20]	Block-MTSET-E NoEff-MTSET-I [6,13]	Block-MTSET-E NoEff-MTSET-I [6,13]	Accessible from outside open/closed-state
F375C	NoEff-I [19]	NoEff-I [19]	–	–	D(Cα–Cα) > 14 Å
V376C	NoEff-I [19]	NoEff-I [19]	–	–	D(Cα–Cα) > 14 Å
V377C	NoEff-I [19]	NoEff-I [19]	–	–	D(Cα–Cα) > 14 Å
A378C	NoEff-I [19]	NoEff-I [19]	–	–	D(Cα–Cα) > 14 Å
D379C	NoEff-I [19]	NoEff-I [19]	–	–	D(Cα–Cα) > 14 Å
F380	Poten-I [19]	Block-I [19]	–	–	D(F380Cα–C314Cα) < 8 Å **CuP**: Disulfide bridge
F380C–L356C	NoEff-I [19]	NoEff-I [19]	–	–	D(F380Cα–L356Cα) ≈ 6 Å Disulphide bridge formation
I381C	NoEff-I [19]	NoEff-I [19]	–	–	D(Cα–Cα) > 14 Å
I382C	NoEff-I [19]	NoEff-I [19]	–	–	D(Cα–Cα) > 14 Å
I383C	NoEff-I [19]	NoEff-I [19]	–	–	D(Cα–Cα) > 14 Å
V384C	NoEff-I [19]	NoEff-I [19]	Block-MTSEA-I [15]		D(Cα–Cα) > 14 Å Face central pore
L385C	NoEff-I [19]	NoEff-I [19]	NoEff-MTSEA-I [15]		D(Cα–Cα) > 14 Å
I386C	NoEff-I [19]	NoEff-I [19]	NoEff-MTSEA-I [15]		D(Cα–Cα) > 14 Å
F387C	NoEff-I [19]	NoEff-I [19]	Block-MTSEA-I [15]		D(Cα–Cα) > 14 Å Face central pore
A388C	NoEff-I [19]	NoEff-I [19]	Block-MTSEA-I [15]		D(Cα–Cα) > 14 Å Face central pore
T389C	NoEff-I [19]	NoEff-I [19]	Block-MTSEA-I [15]		D(Cα–Cα) > 14 Å
I390C	NoEff-I [19]	NoEff-I [19]	NoEff-MTSEA-I [15]		D(Cα–Cα) > 14 Å
V391C	Block-I [19]	Block-I [19]	Block-MTSET- I [16] Block-MTSEA-I [16]	NoEff MTSET-I [16] BlockMTSEA-I [16]	D(Cα–Cα) < 14 Å Face central pore
G392C	NoEff-I [19]	NoEff-I [19]	Block-MTSET-I [16] Block-MTSEA-I [15]		D(Cα–Cα) > 14 Å Face central pore
N393C	NoEff-I [19]	NoEff-I [19]	Block-MTSET-I [16] NoEff-MTSEA-I [15]$^{-}$		D(Cα–Cα) > 14 Å
I394C	NoEff-I [19]	NoEff-I [19]	Block-MTSET-I [16]$^{-}$ Block-MTSEA-I [15]	NoEff-MTSET-I [16]	D(Cα–Cα) > 14 Å Face central pore
G395C	Block-I [19]	Block-I [19]	Block-MTSET-I [16]$^{-}$ Block-MTSEA-I [15]		D(Cα–Cα) < 14 Å Face central pore
S396C	NoEff-I [19]	Block-I [19]	Block-MTSET-I [16]$^{-}$ Block-MTSEA-I [15]	Block-MTSET-I [16]	D(Cα–Cα) < 14 Å
S397C			NoEff-MTSET-I [16]$^{-}$ NoEff-MTSEA-I [15]	–	D(Cα–Cα) < 14 Å
I398C	NoEff-I [19]	NoEff-I [19]	Block-MTSET-I [16] NoEff-MTSEA-I [15]	–	D(Cα–Cα) > 14 Å (open) D(Cα–Cα) ≈ 11 Å (closed)
S399C	Block-I [19]	BlockI [19]	Block-MTSET-I [16] Block-MTSEA-I [15]	Block-MTSET-I [16]	D(Cα–Cα) < 14 Å Face central pore
N400C	**NoEff-I** [19]	**Block-I** [19]	–	–	D(Cα–Cα) > 14 Å (open) D(Cα–Cα) ≈ 11 Å (closed)

(*continued on next page*)

Table 1 (*continued*)

Mutant	Cd^{2+}		MTS		Restraint
	Open	Closed	Open	Closed	
M401C	NoEff-I [19]	NoEff-I [19]	–	–	$D(C\alpha–C\alpha) > 14$ Å
N402C	**NoEff-I** [19]	**Block-I** [19]	–	–	$D(C\alpha–C\alpha) > 14$ Å (open)
					$D(C\alpha–C\alpha) \approx 11$ Å (closed)
A403C	**NoEff-I** [19]	**Block-I** [19]	–	–	$D(C\alpha–C\alpha) > 14$ Å (open)
					$D(C\alpha–C\alpha) \approx 11$ Å (closed)
A404C	**NoEf- I** [19]	**Block-I** [19]	–	–	$D(C\alpha–C\alpha) > 14$ Å (open)
					$D(C\alpha–C\alpha) \approx 11$ Å (closed)
R405C	NoEff-I [19]	NoEff-I [19]	–	–	$D(C\alpha–C\alpha) > 14$ Å
A406C	**NoEff-I** [19]	**Block-I** [19]			$D(C\alpha–C\alpha) > 14$ Å (open)
					$D(C\alpha–C\alpha) \approx 11$ Å (closed)
D407C	**NoEff-I** [19]	**Block-I** [19]	–	–	$D(C\alpha–C\alpha) > 14$ Å (open)
					$D(C\alpha–C\alpha) \approx 11$ Å (closed)
F408C	**NoEff-I** [19]	**Block-I** [19]	–	–	$D(C\alpha–C\alpha) > 14$ Å (open)
					$D(C\alpha–C\alpha) \approx 11$ Å (closed)
Q409C	**NoEff-I** [19]	**Block-I** [19]	–	–	$D(C\alpha–C\alpha) > 14$ Å (open)
					$D(C\alpha–C\alpha) \approx 11$ Å (closed)
A410C	NoEff-I [19]	NoEff-I [19]			$D(C\alpha–C\alpha) > 14$ Å
I412C	NoEff-I [19]	NoEff-I [19]	–	–	$D(C\alpha–C\alpha) > 14$ Å
A413C	**Block-I** [19]	**Poten-I** [19]			$D(C\alpha–C\alpha) > 14$ Å
A414C	**NoEff-I** [19]	**Block-I** [19]	–	–	$D(C\alpha–C\alpha) > 14$ Å (open)
					$D(C\alpha–C\alpha) \approx 11$ Å (closed)
I415C	NoEff-I [19]	NoEff-I [19]	–	–	$D(C\alpha–C\alpha) > 14$ Å
L416C	NoEff-I [19]	NoEff-I [19]	–	–	$D(C\alpha–C\alpha) > 14$ Å
Q417C	**NoEff-I** [19]	**Block-I** [19]			$D(C\alpha–C\alpha) > 14$ Å (open)
					$D(C\alpha–C\alpha) \approx 11$ Å (closed)
Y418C	Block-I [19]	Block-I [19]	–	–	$D(C\alpha–C\alpha) > 14$ Å (open)
					$D(C\alpha–C\alpha) \approx 11$ Å (closed)
M419C	NoEff-I [19]	NoEff-I [19]	–	–	$D(C\alpha–C\alpha) > 14$ Å
H420C	NoEff-I [19]	NoEff-I [19]			$D(C\alpha–C\alpha) > 14$ Å
F421C	NoEff-I [19]	NoEff-I [19]	–	–	$D(C\alpha–C\alpha) > 14$ Å
R422C	**NoEff-I** [19]	**Block-I** [19]	–	–	$D(C\alpha–C\alpha) > 14$ Å (open)
					$D(C\alpha–C\alpha) \approx 11$ Å (closed)

Distance restraints always refer to opposite Cα in the tetramer, unless specified. Accessibilities patterns were used to constraint the P-helix orientation in agreement with [13]. The first, second, third and fourth bracket refer to the blue, gray, yellow and red color coding in the figures. Abbreviation details: No Eff: no effect; Block: irreversible blockage of the current; E and I: measurements carried out with the reagents in the extracellular and intracellular sides of the membrane, respectively; Poten: current potentiation; MTS: methylsulfonate agents – MTSET, MTSEA, MTSES – (see text). Experimental information: The CNGA1 channel contained native cysteines [6]; experiments performed in tandem construct of CNGA1 (with native cysteines) channels where cysteine mutants were introduced in only one of the tandem component [13]; experiments performed in a cysteine-free CNGA1 channel from bovine rods [15,16]; the CNGA1 channel contained native cysteines [18–20].

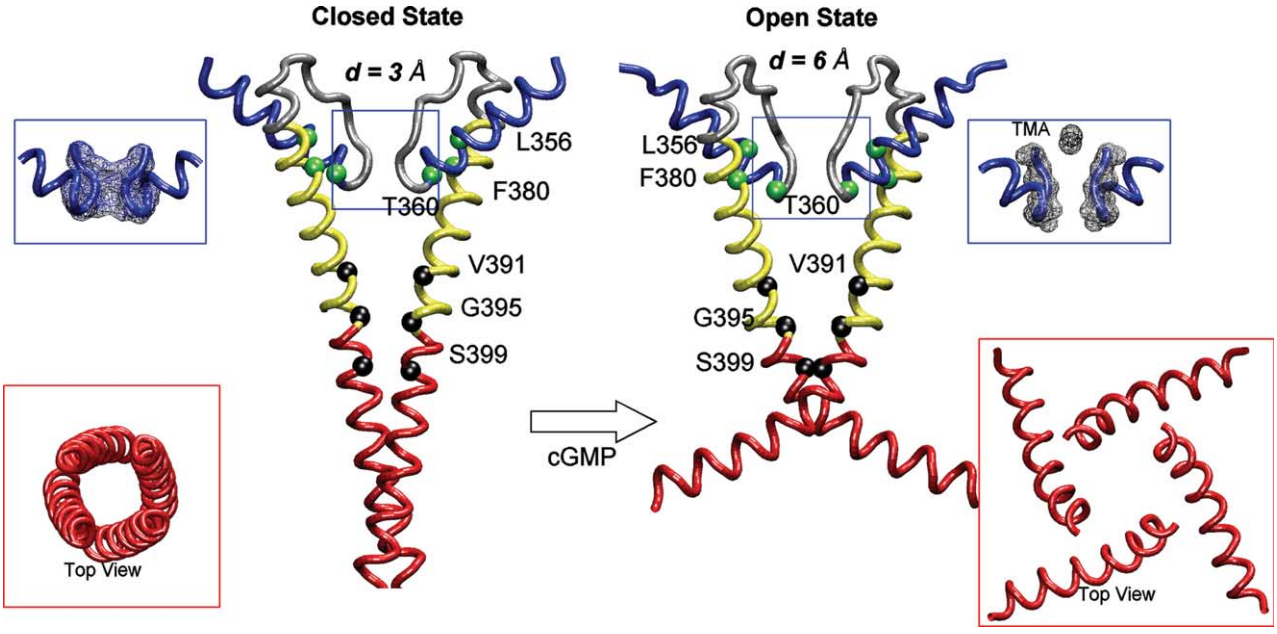

Fig. 2. Structural models [31] of S6, the P loop of the transmembrane domain along with the N-term@C-linker in the closed and open states. Only two opposite subunits are shown for the sake of clarity. The structures were obtained by homology modelling (see Fig. 1B) by using Modeller6v2 [32] with the inclusion of the spatial constraints in Table 1. Selected residues's Cα are shown. *d* is the shortest distance between opposite Cα's in the pore. Insets: (i) Detail of the central P-Helix-Loop region (able to permeate trimethylammonium ion (TMA^+) only in the open conformation) (Blue). Also here only two opposite subunits are shown. (ii) Top view of the N-term@C-linker (Red).

In conclusion, the initial event of cyclic nucleotide binding is transmitted to the pore walls by a remarkable and sophisticated coupling of conformational changes spanning throughout the entire cytoplasmic and transmembrane domains of the channel.

Acknowledgments: We thank Glaxo-Wellcome UK and the Human Frontier Program for financial support (HFSP Program Grant RGP0054/2002). Anna Tramontano is acknowledged for critically discussing the research presented here.

References

[1] Hille, B. (2001) Ionic Channels of Excitable Membranes, Sinaver Associate, Sunderland, MA.
[2] Giorgetti, A. and Carloni, P. (2003) Molecular modelling of ion chanels: structural predictions. Curr. Opin. Chem. Biol. 7 (1), 150–156.
[3] Capener, C.E, Kim, H.J., Arinaminpathy, Y. and Sansom, M.S. (2002) Ion channels: structural bioinformatics and modelling. Hum. Mol. Genet. 11 (20), 2425–2433.
[4] Simoes, M., Garneau, L., Klein, H., Banderali, U., Hobeila, F., Roux, B., Parent, L. and Sauve, R. (2002) Cysteine mutagenesis and computer modeling of the S6 region of an intermediate conductance IKCa channels. J. Gen. Physiol. 120 (1), 99–116.
[5] Kaupp, U.B., Niidome, T., Tanabe, T., Terada, S., Bonigk, W., Stuhmer, W., Cook, N.J., Kangawa, K., Matsuo, H. and Hirose, T. (1989) Primary structure and functional expression from complementary DNA of the rod photoreceptor cyclic GMP-gated channel. Nature 342, 762–766.
[6] Becchetti, A., Gamel, K. and Torre, V. (1999) Cyclic nucleotide-gated channels. Pore topology studied through the accessibility of reporter cysteines. J. Gen. Physiol. 114, 377–392.
[7] Sesti, F., Eismann, E., Kaupp, U.B., Nizzari, M. and Torre, V. (1995) The multi-ion nature of the cGMP-gated channel from vertebrate rods. J. Physiol. 487 (Pt. 1), 17–36.
[8] Johnson, J. and Zagotta, W.N. (2001) Rotation movement during cyclic nucleotide-gated channel opening. Nature 412, 917–921.
[9] Matulef, K., Flynn, G.E. and Zagotta, W.N. (1999) Molecular rearrangements in the ligand-binding domain of cyclic nucleotide-gated channels. Neuron 24, 443–452.
[10] Jiang, Y., Lee, A., Chen, J., Cadene, M., Chait, B.T. and MacKinnon, R. (2002) The open pore conformation of potassium channels. Nature 417, 523–526.
[11] Zhou, Y., Morais-Cabral, J.H., Kaufman, A. and MacKinnon, R. (2001) Chemistry of ion coordination and hydration revealed by a K+ channel-Fab complex at 2.0 Å resolution. Nature 414, 43–48.
[12] Zagotta, W.N., Olivier, N.B., Black, K.D., Young, E.C., Olson, R. and Gouaux, E. (2003) Stuctural basis for modulation and agonist specificity of HCN pacemakers channels. Nature 425, 200–205.
[13] Liu, J. and Siegelbaum, S.A. (2000) Change of pore helix conformational state upon opening of cyclic nucleotide-gated channels. Neuron 28, 899–909.
[14] Flynn, G.E. and Zagotta, W.N. (2001) Conformational changes in S6 coupled to the opening of cyclic nucleotide-gated channels. Neuron 30, 689–698.
[15] Flynn, G.E. and Zagotta, W.N. (2001) A cysteine scan of the inner vestibule of cyclic nucleotide-gated channels reveals architecture and rearrangement of the pore. J. Gen. Physiol 121, 563–582.
[16] Flynn, G.E., Johnson, J.P. and Zagotta, W.N. (2001) Cyclic nucleotide-gated channels: shedding light on the opening of a channel pore. Nat. Rev. Neurosci. 2, 643–651.
[17] Johnson, J.P. and Zagotta, W.N. (2001) Rotational movement during cyclic nucleotide-gated channel opening. Nature 412, 917–921.
[18] Mazzolini, M., Codega, P., Nair, A.V, Giorgetti, A., Torre, V. Conformational changes in the S6 domain of CNGA1 channels probed by intracellular Cd(II), J. Gen. Physiol., submitted.
[19] Nair, A.V., Mazzolini, M., Codega, P., Giorgetti, A., Torre, V. Conformational changes in the pore of CNGA1 channels during gating, revealed by electrophysiological experiments with mutant channels, J. Gen. Physiol., submitted.
[20] Becchetti, A. and Roncaglia, P. (2000) Cyclic nucleotide-gated channels: intra and extracellular accessibility to Cd^{2+} of substituted cysteine residues within the P-loop. Pflugers Arch. 440, 556–565.
[21] Rothberg, B., Shin, K., Phale, P. and Yellen, G. (2002) Voltage-controlled gating at the intracellular entrance to a hyperpolarization-activated cation channel. J. Gen. Physiol. 119 (2002), 83–91.
[22] Berman, H.M., Westbrook, J., Feng, Z., Gilliland, G., Bhat, T.N., Weissig, H., Shindyalov, I.N. and Bourne, P.E. (2000) The Protein Data Bank. Nucleic Acids Res. 28, 235–242.
[23] The hypothesis that the presence of a close proximity between opposite H420 residues, as inferred in [8] by Ni^{2+} binding, is not consistent with the whole set of (about 22 experiments) data on the C-linker from N400C to R442C and it is therefore not included here.
[24] Akabas, M.H., Stauffer, D.A., Xu, M. and Karlin, A. (1992) Acetylcholine receptor channel structure probed in cysteine-substitution mutants. Science 258, 307–310.
[25] Because the topology of MthK is similar to that of KcsA, we have attempted using the former as a template for the open configuration. The MthK based constructs from Cd^{2+} adducts (Table 1) resulted in extremely large rearrangements (more than 10 Å), while causing relatively small rearrangements (overall RMSD of 3 Å) (Fig. 2) in the KcsA-based model. Thus, MthK was not considered any further.
[26] Webster, S.M., del Camino, D., Dekker, J.P. and Yellen, G. (2004) Intracellular gate opening in Shaker K+ channels defined by high-affinity metal bridges. Nature 428, 864–868.
[27] Goulding, E.H., Tibbs, G.R., Liu, D. and Siegelbaum, S.A. (1993) Role of H5 domain in determining pore diameter and ion permeation through cyclic nucleotide-gated channels. Nature 364, 61–64.
[28] Bucossi, G., Eismann, E., Sesti, F., Nizzari, M., Seri, M., Kaupp, U.B. and Torre, V. (1996) Time-dependent current decline in cyclic GMP-gated bovine channels caused by point mutations in the pore region expressed in *Xenopus* oocytes. J. Physiol. 493 (Pt. 2), 409–418.
[29] Laio, A. and Torre, V. (1999) Physical origin of selectivity in ionic channels of biological membranes. Biophys. J. 76, 129–148.
[30] Doyle, D.A., Morais-Cabral, J., Pfuetzner, R.A., Kuo, A., Gulbis, J.M., Cohen, S.L., Chait, B.T. and MacKinnon, R. (1998) The structure of the potassium channel: molecular basis of K+ conduction and selectivity. Science 280, 69–77.
[31] The final models can be found in the following web address: www.sissa.it/sbp/web/research/biomolecular_simulations/pdbfiles/.
[32] Sanchez, R. and Sali, A. (1997) Advances in comparative protein-structure modelling. Curr. Opin. Struct. Biol. 7, 206–214.